



Displaced vertex and disappearing track signatures in type-III seesaw

Sudip Jana^{1,a}, Nobuchika Okada^{2,b}, Digesh Raut^{3,c}

¹ Max-Planck-Institut für Kernphysik, Saupfercheckweg 1, 69117 Heidelberg, Germany

² Department of Physics and Astronomy, University of Alabama, Tuscaloosa, AL 35487, USA

³ Washington College, Chestertown, MD 21620, USA

Received: 4 September 2020 / Accepted: 28 September 2022 / Published online: 19 October 2022
© The Author(s) 2022

Abstract We investigate a prospect of probing the type-III seesaw neutrino mass generation mechanism at various collider experiments by searching for a disappearing track and a displaced vertex signature originating from the decay of $SU(2)_L$ triplet fermion (Σ). Since Σ is primarily produced at colliders through the electroweak gauge interactions, its production rate is uniquely determined by its mass. We find that a Σ particle produces a disappearing track signature from the decay of its charged component, which can be searched at the HL-LHC. Furthermore, we show that if the lightest observed neutrino has a mass of around 10^{-9} eV, the neutral component of Σ can be discovered at the proposed MATH-USLA detector. We also show that the charged component of Σ can be potentially be observed at FCC-he as a displaced vertex signature.

1 Introduction

The Standard Model (SM) of particle physics is a tremendously successful theory, but it is incomplete in its current form. Among its various shortcomings, we here focus on the fact that the SM offers no explanation about the origin of the tiny observed masses of the observed neutrinos [1–6]. One of the most appealing scenario to naturally generate the tiny neutrino masses is the seesaw mechanism, namely, type-I seesaw [7–11], type-II seesaw [12–16] and type-III seesaw [17], which effectively generates the lepton number violating dimension five operator $\mathcal{O}_5 = \frac{c}{\Lambda} LLHH$ at low energies, where Λ is the seesaw scale.

In this paper, we focus on the type-III seesaw, where in addition to the SM particles, at least two $SU(2)_L$ triplet fermions (Σ) with zero hypercharge are introduced [17]. For example, if the type-III seesaw mechanism is incorporated in the grand unified theory (GUT) framework, the triplet fermion mass M_Σ are of the intermediate scale [17–21].¹ However, the type-III seesaw scenario with $M_\Sigma \simeq \mathcal{O}(1)$ TeV is also technically natural. Unlike GUT scenarios, the latter can be explored at collider experiments. See, for example, Refs. [22–29]. The CMS [30] and the ATLAS collaborations [31] for the Large Hadron Collider (LHC) have carried out a dedicated search for an $SU(2)_L$ triplet fermion of the type-III seesaw. Particularly, their search focuses on the prompt decay of the neutral (Σ^0) and the charged (Σ^\pm) components of Σ produced via an intermediate electroweak gauge bosons that yields two final-state leptons (electrons or muons) of different flavors and charge combinations accompanied by at least two jets. Assuming flavor-universal branching fractions of $\Sigma^{0,\pm}$ into different lepton flavors, $M_\Sigma < 840$ GeV is excluded [30].

We explore an interesting possibility that $\Sigma^{0,\pm}$ are long-lived and evade the prompt decay searches at the LHC, thereby explaining the null results from the LHC experiments. The mass-splitting between Σ^\pm and Σ^0 is small, $\mathcal{O}(10^2)$ MeV, such that the pion/SM leptons produced in Σ^\pm decay to Σ^0 are soft and very challenging to reconstruct at the LHC (a proton and proton (pp)-collider) due to a large hadronic background. If the neutral fermion Σ^0 lives long enough to pass through the detector undetected, the observed track of the charged Σ^\pm disappear after they decay inside the detector. However, a detailed analysis of such a scenario has not been considered in the literature. We will show that this

^a e-mail: sudip.jana@mpi-hd.mpg.de

^b e-mail: okadan@ua.edu

^c e-mail: draut2@washcoll.edu (corresponding author)

¹ For a discussion of GUT scenario with $M_\Sigma \lesssim \mathcal{O}(1)$ TeV, see Ref. [25].

so-called disappearing track signature can be the primary discovery mode of the long-lived Σ^\pm at the LHC and the future HL-LHC. For comparison, a dedicated disappearing track search for chargino in supersymmetric models, whose production and decay mechanism is very similar to Σ^\pm , has already led to a very stringent bound [32].

For a long-lived charge neutral particle, its decay vertex is located away from the collision point. This so-called displaced vertex signature is a very clean with almost zero SM background. The current status of the displaced vertex searches at the LHC can be found in Refs. [33–49]. We expect a dramatic improvement in the search for the displaced vertex at future collider experiments, such as the proposed MAssive Timing Hodoscope for Ultra Stable neutral pArticles (MATHUSLA) experiment [50] of the HL-LHC,² the Large Hadron electron Collider (LHeC) [53] and the Future Circular electron-hadron Colliders (FCC-he) [54]. The MATHUSLA detector is an external detector purposed to detect the decay of long-lived particles which have escaped the detection at the LHC such as Σ^0 of the type-III seesaw.³ Being purposefully placed far away from the LHC, this experiment is ideal to search for a long-lived Σ^0 . In fact, we find that MATHUSLA can discover Σ^0 . Compared to the LHC, electron and proton (ep)-colliders such as the LHeC and FCC-he have cleaner environments because they are free from large hadronic background and pile-up events at higher luminosities. This enables explicit reconstruction of the soft final states in Σ^\pm decay to Σ^0 for a displaced vertex signature. See, for example, Ref. [55] for the discussion of Higgsino search prospect at the LHeC and FCC-he. Because of the asymmetric beam setup of the ep -colliders, the charged Higgsinos produced at these colliders are boosted and effectively have a longer lifetime in the lab frame. Thus, ep -collider can access lifetimes many orders of magnitude shorter than the pp -colliders. We will show that FCC-he can also probe the type-III seesaw mechanism.

In the following, we will show that the disappearing track and displaced vertex signatures that arise from the decay of $\Sigma^{\pm,0}$ in type-III seesaw can be probed at HL-LHC, MATHUSLA, and FCC-he experiments. This work is organized as follows: In Sect. 2, we introduce the type-III seesaw mechanism and discuss the neutrino mass generation mechanism. In Sect. 3, we study the production of $\Sigma^{\pm,0}$ at HL-LHC and FCC-he, and also calculate their decay lengths. After dis-

cussing the bounds from the disappearing track search at the LHC experiment as well its search prospect at the HL-LHC, we examine in Sect. 5 the prospect of observing the displaced vertex signal of $\Sigma^{\pm,0}$ decay at MATHUSLA, and FCC-he. Finally, we present our conclusion in Sect. 6.

2 The type-III seesaw

We consider the extension of the SM with three generation of $SU(2)_L$ triplet (right-handed) fermions, Σ_i ($i = 1, 2, 3$), and the Lagrangian is given by

$$\mathcal{L}_\Sigma = \text{Tr} [\bar{\Sigma}_i \not{D} \Sigma_i] - \left(\frac{1}{2} M_\Sigma^{ij} \text{Tr} [\bar{\Sigma}_i^c \Sigma_j] + \text{h.c.} \right) - \left(Y_\Sigma^{ij} \bar{L}_i \Sigma_j H + \text{h.c.} \right), \quad (2.1)$$

where D is the covariant derivative for Σ_i , M_Σ^{ij} are Majorana masses of the triplet fermions, Y_Σ^{ij} are the Dirac-type Yukawa couplings, $L_i \equiv (v_i, l_i)^T$ is the left-handed SM $SU(2)_L$ lepton doublet, $H \equiv (H^0, H^-)^T = \left((v + h + i\eta)/\sqrt{2}, H^- \right)^T$ and $v = 246$ GeV. The $SU(2)_L$ triplet fermion contains charged (Σ^\pm) and charge neutral (Σ^0) components which can be expressed as

$$\Sigma_i = \begin{pmatrix} \Sigma_i^0/\sqrt{2} & \Sigma_i^+ \\ \Sigma_i^- & -\Sigma_i^0/\sqrt{2} \end{pmatrix}, \quad (2.2)$$

and its conjugate is given by $\Sigma_i^c \equiv C \bar{\Sigma}_i^T$, where C denotes the charge conjugation operator.

Let us first consider the masses of Σ_i^\pm and Σ_i^0 . Although their masses are degenerate at the tree-level, radiative corrections induced by the electroweak gauge boson loops remove the degeneracy and generate mass-splitting between Σ_i^\pm and Σ_i^0 . The resulting mass difference (ΔM_i) at the one-loop order is given by [67]

$$\Delta M_i = \frac{\alpha_2 m_{\Sigma_i}}{4\pi} \left[f \left(\frac{M_W}{m_{\Sigma_i}} \right) - \cos^2 \theta_W \times f \left(\frac{M_Z}{m_{\Sigma_i}} \right) \right], \quad (2.3)$$

where $\alpha_2 = 0.034$, $\cos^2 \theta_W \simeq 0.769$ [68], the function f is defined as

$$f(r) = r \left[2r^3 \ln r - 2r + (r^2 - 4)^{1/2} (r^2 + 2) \ln A \right] / 2, \quad (2.4)$$

with $A = (r^2 - 2 - r\sqrt{r^2 - 4})/2$. We show ΔM_i as a function of m_{Σ_i} in Fig. 1. The dashed line denotes the π

The Yukawa couplings between H and Σ generate mass-mixings between $\Sigma^{0,\pm}$, ν_ℓ and ℓ_L . The mass matrices involving the charged fermion states, M_\pm in (l^\pm, Σ^\pm) basis and

² Other dedicated displaced vertex search experiments at the LHC such as FASER [51] and the proposed Codex-b (see, for example, Ref. [52]) specialize in search of long-lived neutral particle with mass of a few GeV or smaller which are created from the decay of mesons that are copiously produced at the LHC. Compared to FASER and Codex-b, MATHUSLA has the best search reach because of its large detector volume. For comparison, see, for example, Ref. [52].

³ Such a prospect for type-I seesaw scenario at MATHUSLA experiment has been investigated in Refs. [56–66].

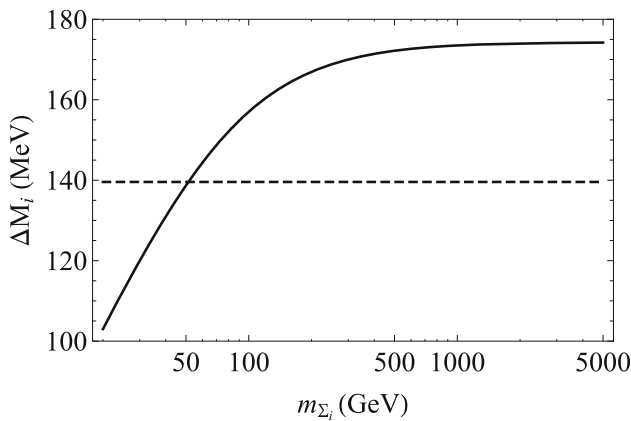


Fig. 1 The mass-splitting between Σ^\pm and Σ^0 induced by radiative corrections as a function of m_Σ . Dashed line denotes the π meson mass

neutral fermion states, M_0 in (ν, Σ^0) basis, are expressed as

$$M^\pm = \begin{pmatrix} m_{\ell^\pm} & -\sqrt{2}m_D \\ 0 & M_\Sigma \end{pmatrix}, \quad M^0 = \begin{pmatrix} 0 & -m_D \\ -m_D^T & M_\Sigma \end{pmatrix}, \quad (2.5)$$

respectively. Here, m_{ℓ^\pm} is the mass matrix for the SM charged leptons, $m_D^{ij} = Y_\Sigma^{ij} v / \sqrt{2}$ are the components of Dirac type neutrino mass matrix (m_D) and $M_\Sigma = \text{diag}(m_{\Sigma_1}, m_{\Sigma_2}, m_{\Sigma_3})$ is the Majorana mass matrix for the triplet fermions. We have fixed the mass eigenvalues of the charged and the neutral components of each triplets to be the same because of the tiny mass-splitting between them. Equation (2.5) shows that the mixings between heavy triplet and light SM states in both the neutral and the charged fermion sectors are of the same order $m_D M_\Sigma^{-1}$. In the following, we will focus on the mixing in the neutral sector which generates the observed neutrino masses. The Feynman diagram for the type-III seesaw is shown in Fig. 2. The light neutrino mass matrix is generated as

$$m_\nu \simeq -m_D (M_\Sigma)^{-1} m_D^T. \quad (2.6)$$

We can express the neutrino flavor eigenstate (ν) as $\nu \simeq \mathcal{N} \nu_m + \mathcal{R} N_m$, where ν_m (Σ_m) are light (heavy) mass eigenstates, $\mathcal{R} = m_D (M_\Sigma)^{-1}$, $\mathcal{N} = \left(1 - \frac{1}{2} \mathcal{R}^* \mathcal{R}^T\right) U_{\text{MNS}} \simeq U_{\text{MNS}}$. The neutrino mass mixing matrix U_{MNS} diagonalizes the light neutrino mass matrix as follows:

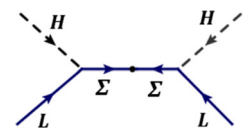
$$U_{\text{MNS}}^T m_\nu U_{\text{MNS}} = D_\nu = \text{diag}(m_1, m_2, m_3), \quad (2.7)$$

where

$$U_{\text{MNS}} = \begin{pmatrix} c_{12}c_{13} & c_{12}c_{13} & s_{13}e^{-i\delta} \\ -s_{12}c_{23} - c_{12}s_{23}s_{13}e^{i\delta} & c_{12}c_{23} - s_{12}s_{23}s_{13}e^{i\delta} & s_{23}c_{13} \\ s_{12}c_{23} - c_{12}c_{23}s_{13}e^{i\delta} & -c_{12}s_{23} - s_{12}c_{23}s_{13}e^{i\delta} & c_{23}c_{13} \end{pmatrix} \begin{pmatrix} 1 & 0 & 0 \\ 0 & e^{-i\rho_1} & 0 \\ 0 & 0 & e^{-i\rho_2} \end{pmatrix}. \quad (2.8)$$

In this work, for simplicity, we set the Majorana CP -phases $\rho_{1,2} = 0$ while we use the best fit values for neutrino masses,

Fig. 2 Tree-level neutrino mass diagram for type-III seesaw mechanism



mixing angles ($c_{ij} \equiv \cos \theta_{ij}$ and $s_{ij} \equiv \sin \theta_{ij}$) and the Dirac CP -phase (δ) from NuFIT's global analysis [69] of neutrino oscillation data. Their values depend on the observed neutrino mass hierarchy, namely, normal hierarchy (NH), $m_1 < m_2 < m_3$, and inverted hierarchy (IH), $m_3 < m_1 < m_2$. For the NH (IH), the best fit central values are $\theta_{12} \simeq 33.4^\circ$ (33.5°), $\theta_{23} \simeq 49.2^\circ$ (49.3°), $\theta_{13} \simeq 8.57^\circ$ (8.60°), $\delta \simeq 197^\circ$ (282°), $\Delta m_{21}^2 \simeq m_2^2 - m_1^2 = 7.42(7.42) \times 10^{-5} \text{ eV}^2$, and $m_{32}^2 \simeq m_3^2 - m_2^2 = 2.51(-2.50) \times 10^{-3} \text{ eV}^2$, respectively.

From Eqs. (2.6) and (2.7), the Dirac mass matrix can be parameterized as [70]

$$im_D = U_{\text{MNS}}^* \sqrt{D_\nu} O \sqrt{M_\Sigma}, \quad (2.9)$$

where $\sqrt{D_\nu} = \text{diag}(\sqrt{m_1}, \sqrt{m_2}, \sqrt{m_3})$, $\sqrt{M_\Sigma} = \text{diag}(\sqrt{m_{\Sigma_1}}, \sqrt{m_{\Sigma_2}}, \sqrt{m_{\Sigma_3}})$ and O is a 3×3 orthogonal matrix. A general 3×3 orthogonal matrix O is given by

$$O = \begin{pmatrix} 1 & 0 & 0 \\ 0 & \cos \theta_1 & \sin \theta_1 \\ 0 & -\sin \theta_1 & \cos \theta_1 \end{pmatrix} \begin{pmatrix} \cos \theta_2 & 0 & \sin \theta_2 \\ 0 & 1 & 0 \\ -\sin \theta_2 & 0 & \cos \theta_2 \end{pmatrix} \\ \times \begin{pmatrix} \cos \theta_3 & \sin \theta_3 & 0 \\ -\sin \theta_3 & \cos \theta_3 & 0 \\ 0 & 0 & 1 \end{pmatrix}, \quad (2.10)$$

where $\theta_{1,2,3}$ are generally complex valued.

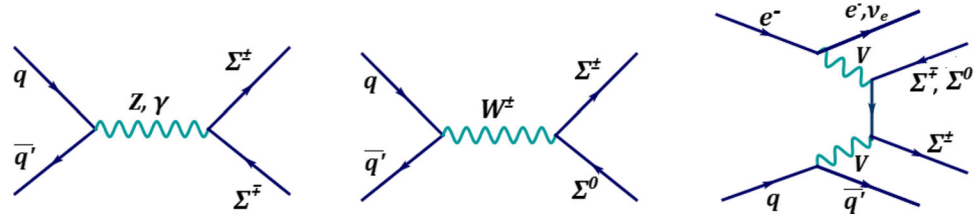
3 Production and search for fermion triplets at current and future colliders

Let us discuss the production of $\Sigma^{0,\pm}$ at various collider experiments. Since Σ is an $SU(2)_L$ triplet, in the type-III seesaw scenario, $\Sigma^{0,\pm}$ are produced at colliders through their electroweak gauge interactions as shown in Fig. 3. All these processes only involve SM gauge interactions, and therefore $\Sigma^{0,\pm}$ production cross sections are solely determined by the triplet mass (m_Σ).

The Drell–Yan processes dominate the Σ production at a pp -collider such as the LHC. The singly charged fermion Σ^\pm is pair-produced from a $q\bar{q}$ fusion through the s -channel Z/γ exchange as shown in the left diagram of Fig. 3. Similarly,

the s -channel W^\pm exchange produces Σ^\pm and Σ^0 as shown in the middle diagram of Fig. 3. The Σ^\pm can also be pair-

Fig. 3 Representative Feynman diagrams for the production of Σ^\pm and Σ^0 at colliders



produced via vector boson-fusion process in association with two forward jets (its diagram is similar to the right diagram in Fig. 3). Despite a large production rate, this process suffers from larger QCD background due to the forward jets activity and is sub-dominant⁴ compared to the Drell–Yan processes. Hence, we do not include vector boson-fusion process in our LHC analysis. On the other hand, the vector boson-fusion process shown in the right diagram of Fig. 3 dominates the production at the ep -colliders such as FCC-he. Because of the clean (low pile-up) environment of the ep -colliders, as we have discussed earlier, the FCC-he can probe much shorter lifetimes and are complementary to LHC disappearing track search of Σ^\pm decay. The FCC-he will look for the displaced vertex signature from Σ^\pm decay.

We generate the signal sample for fermion triplet with MADGRAPH5AMC@NLO [74] event-generator to evaluate the production cross section of the $\Sigma^{0,\pm}$ at LHC and FCC-he. Our results are shown in Fig. 4 as a function of m_Σ . In the left panel of Fig. 4, we show the production cross section for the processes at the LHC with the center of mass energy $\sqrt{s} = 13$ TeV. In the right panel of Fig. 4, we show the production cross section for the FCC-he collider, respectively, where the proton and e^- beam energy is set to be 50 TeV and 60 TeV, respectively.

We conclude this section by discussing the prospect of probing the type-III seesaw at various current and planned collider experiments. After being produced at the collider, the triplet fermion Σ decays to the SM particles. The type of signal observed at collider depends on the lifetime ($c\tau$) of the charged (Σ^\pm) and the neutral component (Σ^0) of the triplet fermion. The Feynman diagrams representing their decays are shown in Figs. 5 and 6. Both Σ^0 and Σ^\pm decay to $W^\pm/Z/h$ plus SM leptons (hereafter, WZh) while Σ^\pm can additionally decay to Σ^0 in association with soft pions/SM leptons. The CMS experiment have searched for $\Sigma^{\pm,0}$ decaying promptly to WZh inside the LHC detector ($c\tau \lesssim 10$ m) and excluded the triplet mass $m_\Sigma < 840$ GeV [30]. As we will show in the next section, Σ^0 can have lifetime $c\tau > 10$ m and hence evade prompt-detection at the LHC. In this case, the CMS prompt-search bound is not applicable. The soft pion/SM lepton accompanying the long-lived Σ_0 in Σ^\pm decay also avoid prompt-detection at the LHC. However, as we have discussed earlier, in this case the LHC and HL-

LHC can search for the disappearing track signature [75, 76]. Meanwhile, if the lifetime of Σ^0 is around 100 m, we will show that MATHUSLA detector can discover it. Additionally, the clean (low pile up) environment at the proposed ep -collider such as the FCC-he enable the reconstruction of the displaced pion and SM leptons from the Σ^\pm decay. We will also examine the prospect of FCC-he to search for the displaced track signature of a decaying long-lived Σ^\pm . Besides these, other interesting scenarios are also possible in the type-III seesaw. For example, $\Sigma^{0,\pm}$ could all decay non-promptly inside the LHC detector such that one could simultaneously look for a displaced vertex signature from Σ^0 decay and displaced or disappearing track signature from Σ^\pm decay.

4 Branching ratio and decay width of the fermion triplets

The partial decay width of Σ^0 to SM Higgs (h) and gauge bosons (Z , W^\pm) are given by [23, 24]

$$\begin{aligned}\Gamma(\Sigma_i^0 \rightarrow h\nu_\alpha) &= \Gamma(\Sigma_i^0 \rightarrow h\bar{\nu}_\alpha) \\ &= \frac{1}{8} \frac{m_{\Sigma_i}^3}{8\pi} \left(\frac{|R_{\alpha i}|^2}{v^2} \right) \left(1 - \frac{m_h^2}{m_{\Sigma_i}^2} \right)^2, \\ \Gamma(\Sigma_i^0 \rightarrow Z\nu_\alpha) &= \Gamma(\Sigma_i^0 \rightarrow Z\bar{\nu}_\alpha) \\ &= \frac{1}{8} \frac{m_{\Sigma_i}^3}{8\pi} \left(\frac{|R_{\alpha i}|^2}{v^2} \right) \left(1 - \frac{M_Z^2}{m_{\Sigma_i}^2} \right)^2 \left(1 + \frac{2M_Z^2}{m_{\Sigma_i}^2} \right), \\ \Gamma(\Sigma_i^0 \rightarrow W^+\ell_\alpha^-) &= \Gamma(\Sigma_i^0 \rightarrow W^-\ell_\alpha^+) \\ &= \frac{1}{4} \frac{m_{\Sigma_i}^3}{8\pi} \left(\frac{|R_{\alpha i}|^2}{v^2} \right) \left(1 - \frac{M_W^2}{m_{\Sigma_i}^2} \right)^2 \left(1 + \frac{2M_W^2}{m_{\Sigma_i}^2} \right),\end{aligned}\quad (4.1)$$

where $\alpha = e, \mu, \tau$ denotes different lepton flavors and

$$R_{\alpha i} = (m_D)_{\alpha i} (M_\Sigma)^{-1} = U_{\text{MNS}}^* \sqrt{D_\nu} O \sqrt{M_\Sigma} (M_\Sigma)^{-1}.\quad (4.2)$$

Similarly, the partial decay width of Σ^\pm to SM Higgs (h) and gauge bosons (Z , W^\pm) are given by [23, 24]

$$\begin{aligned}\Gamma(\Sigma_i^\pm \rightarrow h\ell_\alpha^\pm) &= \frac{1}{4} \frac{m_{\Sigma_i}^3}{8\pi} \left(\frac{|R_{\alpha i}|^2}{v^2} \right) \left(1 - \frac{m_h^2}{m_{\Sigma_i}^2} \right)^2, \\ \Gamma(\Sigma_i^\pm \rightarrow Z\ell_\alpha^\pm) &= \frac{1}{4} \frac{m_{\Sigma_i}^3}{8\pi} \left(\frac{|R_{\alpha i}|^2}{v^2} \right) \left(1 - \frac{M_Z^2}{m_{\Sigma_i}^2} \right)^2\end{aligned}$$

⁴ Similarly, the photon initiated vector-boson processes [71–73] contribution is sub-dominant.

Fig. 4 The left (right) shows the production cross section of Σ_i^\pm and Σ_i^0 at pp (ep)-collider as a function of its mass m_{Σ_i}

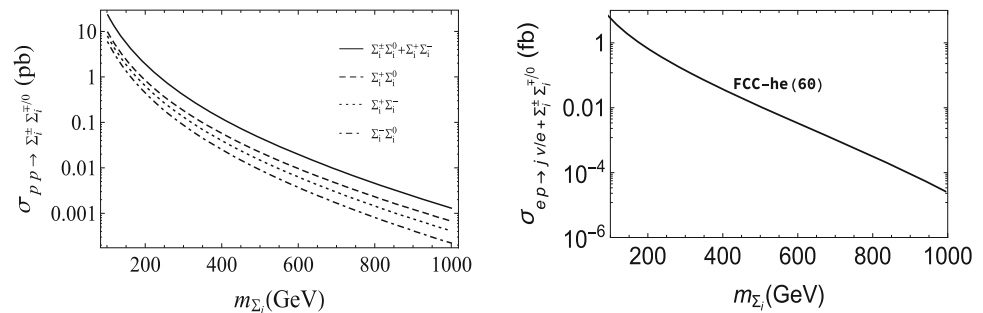


Fig. 5 Representative Feynman diagrams for Σ^0 decay

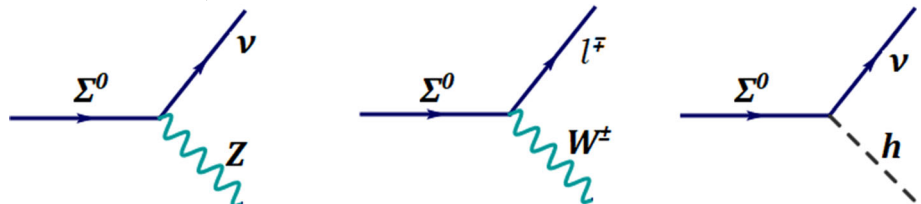
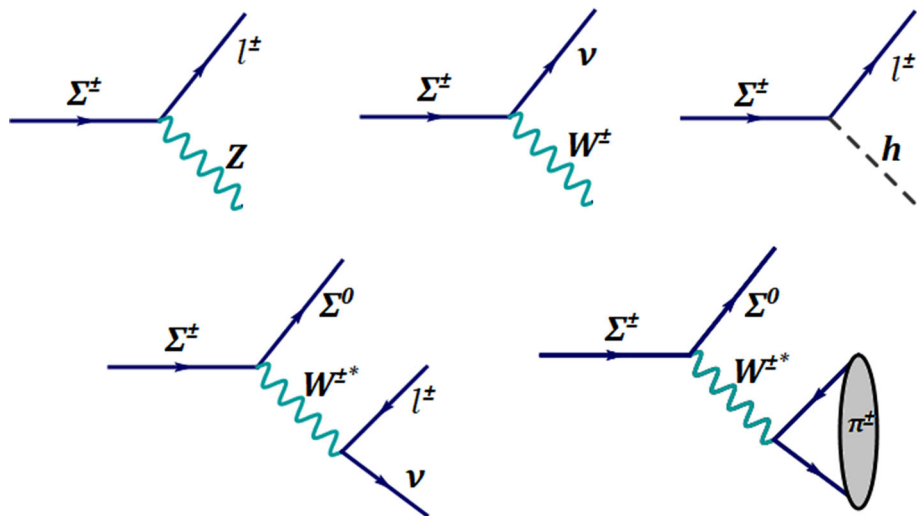


Fig. 6 Representative Feynman diagrams for Σ^\pm decay



$$\begin{aligned} & \times \left(1 + \frac{2M_Z^2}{m_{\Sigma_i}^2}\right), \\ \Gamma(\Sigma_i^\pm \rightarrow W^\pm \bar{\nu}_\alpha) &= \frac{1}{2} \frac{m_{\Sigma_i}^3}{8\pi} \left(\frac{|R_{\alpha i}|^2}{v^2}\right) \left(1 - \frac{2M_W^2}{m_{\Sigma_i}^2}\right)^2 \\ & \times \left(1 + \frac{2M_W^2}{m_{\Sigma_i}^2}\right). \end{aligned} \quad (4.3)$$

Because of the mass-splittings, Σ^\pm can also decay to Σ^0 and pions or light SM leptons. The partial decay widths for these processes are given by [23,24,67]

$$\begin{aligned} \Gamma(\Sigma_i^\pm \rightarrow \Sigma_i^0 \pi^\pm) &= \frac{2G_F^2 V_{ud}^2 \Delta M_i^3 f_\pi^2}{\pi} \sqrt{1 - \frac{m_\pi^2}{\Delta M_i^2}}, \\ \Gamma(\Sigma_i^\pm \rightarrow \Sigma_i^0 e^\pm \bar{\nu}_e) &= \frac{2G_F^2 \Delta M_i^5}{15\pi^3}, \\ \Gamma(\Sigma_i^\pm \rightarrow \Sigma_i^0 \mu^\pm \bar{\nu}_\mu) &= 0.12 \Gamma(\Sigma^\pm \rightarrow \Sigma^0 e^\pm \bar{\nu}_e). \end{aligned} \quad (4.4)$$

The branching ratios of $\Sigma^{0,\pm}$ decaying to WZh and Σ^0 are defined as the ratio of the sum of partial decay widths for each

decay mode to the total decay width of $\Sigma^{0,\pm}$, $\Gamma_{\text{total}}^{\pm,0}$. The decay length of $\Sigma^{0,\pm}$ are given by $c\tau = 1/\Gamma_{\text{total}}^{\pm,0}$. From Eqs. (4.1)–(4.4), all the particle decay widths of $\Sigma^{0,\pm}$ are determined by $m_{1,2,3}$, $m_{\Sigma_{1,2,3}}$, and complex angles $\theta_{1,2,3}$. The observed light neutrino mass spectrum is uniquely determined by the lightest neutrino mass, particularly, m_1 (NH) and m_3 (IH). For the rest of our analysis, we will also fix $m_{\Sigma_{2,3(1,2)}} = 1$ TeV for NH (IH), respectively, which will be justified later. Therefore, the branching ratios and decay length of $\Sigma_i^{0,\pm}$ are determined by five free parameters, namely, $m_{1(3)}$ and $m_{\Sigma_{1(3)}}$ for NH (IH), respectively, and $\theta_{1,2,3}$. We will consider the two cases, $\theta_{1,2,3} = 0$ and $\theta_{1,2,3} \neq 0$, separately.

In Fig. 7, we consider the case with the $\theta_{1,2,3} = 0$ for NH for fixed $m_{\Sigma_1} = 600$ GeV. We show the branching ratio for Σ_i^\pm as a function of m_1 in the top left panel of Fig. 7. The blue (red) lines depict branching ratio for Σ_i^\pm decay to Σ_i^0 (WZh), respectively. The solid, dashed and dotted red/blue lines denote $\Sigma_{1,2,3}^\pm$, respectively, as indicated in the figure legend. The red dashed and dotted lines overlap indistinguishably and indicate that $\Sigma_{2,3}^\pm$ decay 100% to WZh independent

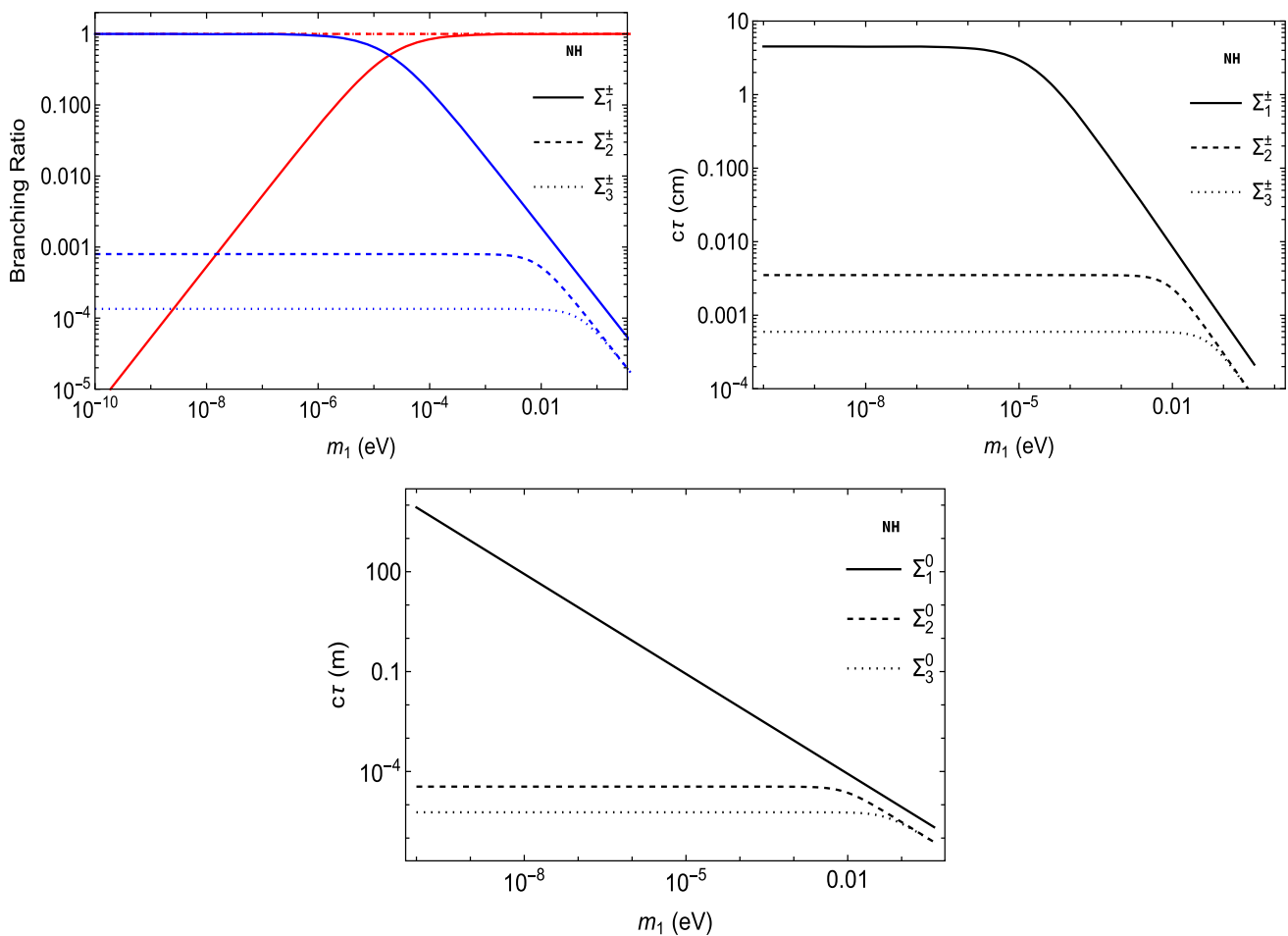


Fig. 7 For NH with $\theta_{1,2,3} = 0$, $m_{\Sigma_1} = 600$ GeV, and $m_{\Sigma_{2,3}} = 1$ TeV, the plots show the branching ratio and decay length of Σ_i^\pm in top left and right panels, respectively, and decay length of Σ_i^0

as a function of lightest observed neutrino mass m_1 in the bottom panel. The blue (red) lines depict branching ratio for Σ_i^\pm decay to Σ_i^0 (WZh)

of m_1 values. On the other hand, Σ_1^\pm decays only to WZh for $m_1 \gg 10^{-4}$ eV. For $m_1 \lesssim 10^{-4}$ eV, Σ_1^\pm 's branching ratio to WZh drops significantly such that Σ_1^\pm decays 100% to Σ_1^0 for $m_1 \ll 10^{-6}$. In the top right panel of Fig. 7, we show the decay length of Σ_i^\pm as a function of m_1 . The solid, dashed and dotted lines denote $\Sigma_{1,2,3}^\pm$, respectively. The decay length for $\Sigma_{1,2,3}^\pm$ all approach constant values for $m_1 \rightarrow 0$. In this limit, the decay length of Σ_1^\pm approaches a constant value because Σ_1^\pm decays to Σ_1^0 independently of light neutrino masses. On the other hand, $\Sigma_{2,3}^\pm$ decays to WZh for any values of m_1 . The WZh partial decay widths of Σ_i^\pm in Eq. (4.3) are all proportional to $|R_{\alpha i}|^2$, which is given by $\Sigma_\alpha |R_{\alpha i}|^2 = m_i/m_{\Sigma_i}$ for $\theta_{1,2,3} = 0$ and is independent of U_{MNS} matrix [56]. Hence, the decay length of Σ_i^\pm is inversely proportional to m_i . For NH ($m_1 < m_2 < m_3$), $m_2 = \sqrt{\Delta m_{21}^2 + m_1^2}$ and $m_3 = \sqrt{m_2^2 + \Delta m_{32}^2}$, both of which approach constant values for $m_1 \rightarrow 0$. Corresponding to the asymptotic values of

$m_{2,3}$, the decay length of $\Sigma_{2,3}^\pm$ also approach constant values in the limit $m_1 \rightarrow 0$. For larger values of $m_1^2 \gg \Delta m_{32}^2$, both $m_{2,3}$ are proportional to m_1 , which explains the decreasing behavior of Σ_i^\pm 's decay lengths for large m_1 values. In the bottom panel of Fig. 7, we show the decay length of Σ_i^0 as a function of m_1 . The solid, dashed and dotted lines denote $\Sigma_{1,2,3}^0$, respectively. The partial decay widths of Σ_i^0 in Eq. (4.1) are all proportional to $|R_{\alpha i}|^2 = m_i/m_{\Sigma_i}$. Therefore, in the limit of $m_1 \rightarrow 0$, the decay length of Σ_1^0 diverges while the decay length of Σ_2^0 and Σ_3^0 approach constant values corresponding to the asymptotic values of $m_{2,3}$.

In Fig. 8, we consider the IH ($m_3 < m_1 < m_2$) case with $\theta_{1,2,3} = 0$, $m_{\Sigma_3} = 600$ GeV and $m_{\Sigma_{1,2}} = 1$ TeV. The line codings of all the figures are the same as Fig. 7. The branching ratio and decay length are determined as a function of m_3 , the lightest mass eigenvalue among the observed neutrinos for the IH case. The top left panel shows that $\Sigma_{1,2}^\pm$, depicted as indistinguishably overlapped solid and dashed

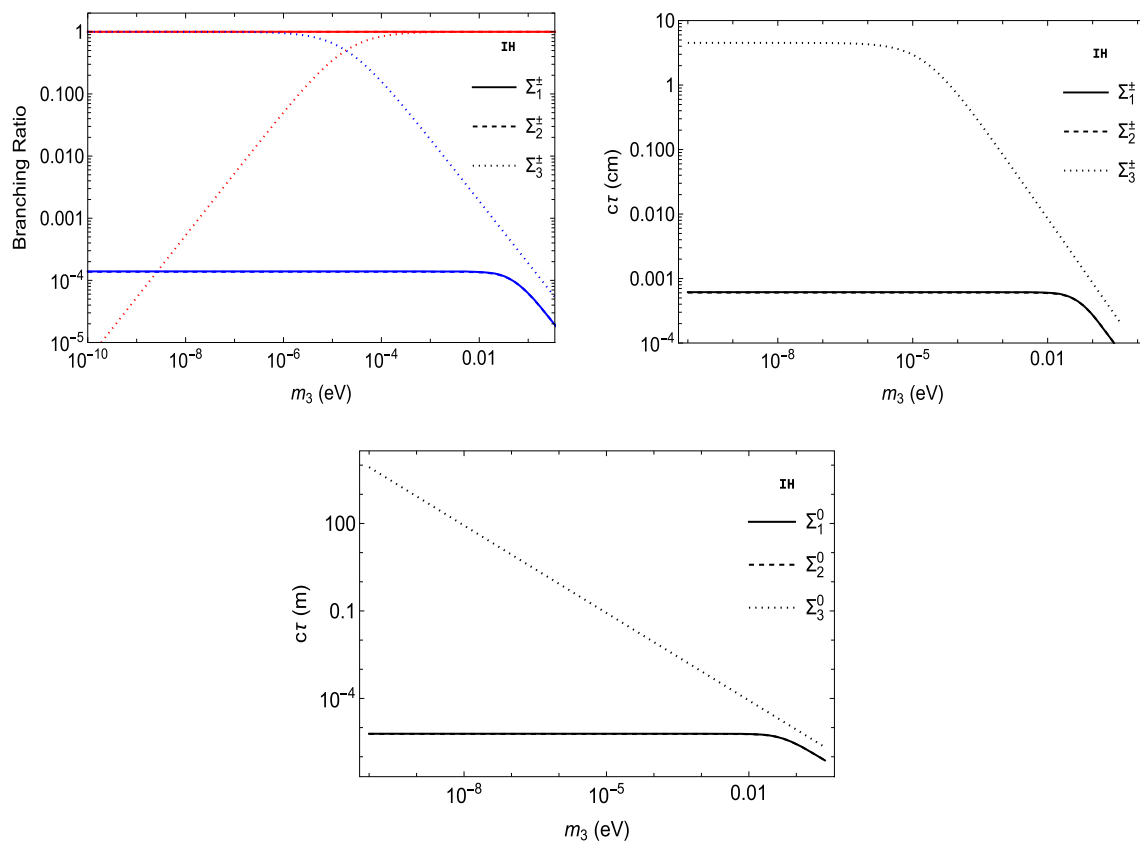


Fig. 8 For NH with $\theta_{1,2,3} = 0$, $m_{\Sigma_3} = 600$ GeV and $m_{\Sigma_{1,2}} = 1$ TeV, the plots show the branching ratio and decay length of $\Sigma_i^{\pm,0}$ as a function of lightest observed neutrino mass m_1 . In the top left and right

panels, respectively, and decay length of Σ_i^0 as a function of lightest observed neutrino mass m_1 in the bottom panel. The blue (red) lines depict branching ratio for Σ_i^{\pm} decay to Σ_i^0 (WZh)

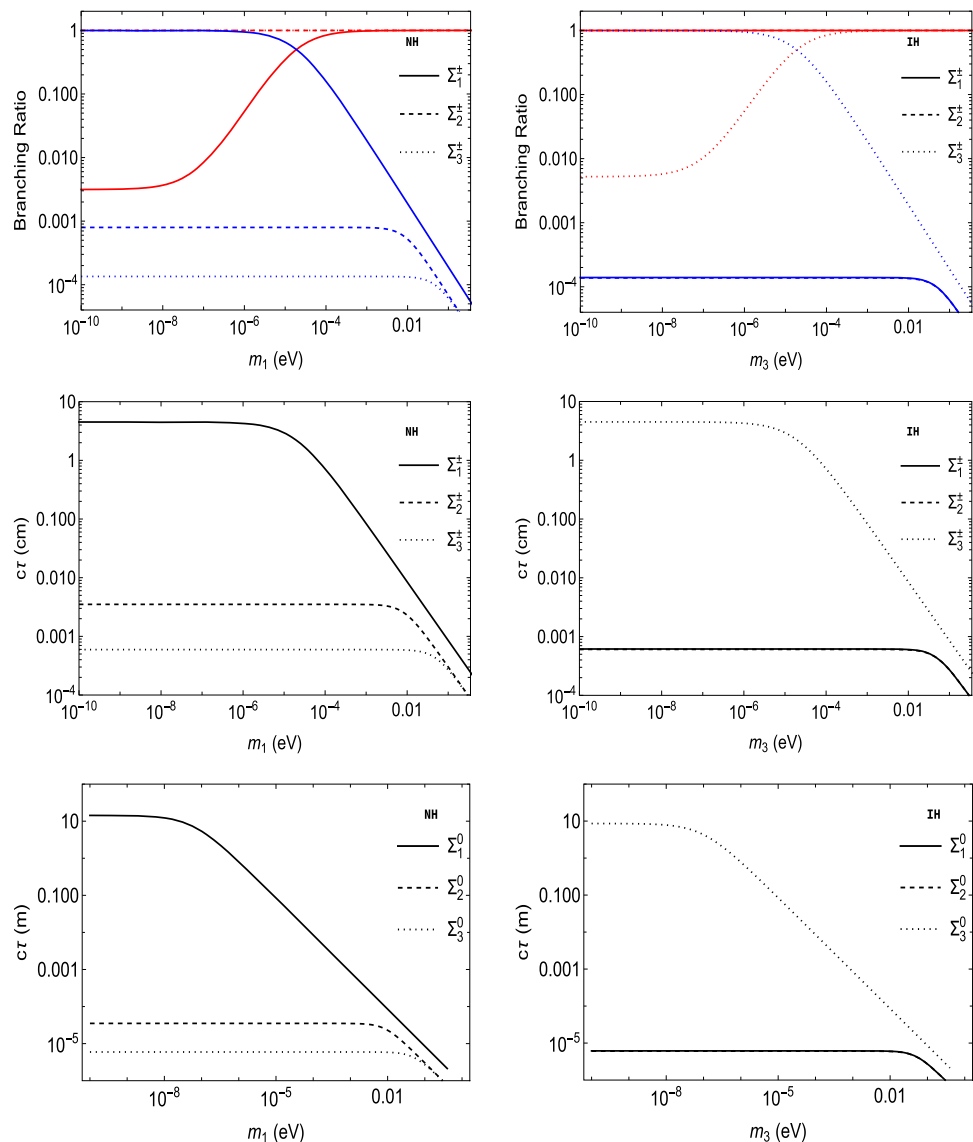
red lines, decay 100% to WZh independently of m_3 values. It also shows that Σ_3^{\pm} decays 100% to Σ_3^0 (WZh) in the limit $m_3 \rightarrow 0$ ($m_3 \rightarrow 0.3$ eV). The discussion to understand the behavior of the decay width of $\Sigma_i^{\pm,0}$ is very much analogous to that of the NH case. For example, the longest decay length is realized for Σ_3^{\pm} and Σ_3^0 corresponding to the lightest neutrino mass in the IH case. The decay length of Σ_3^{\pm} , depicted as indistinguishably overlapped solid and dashed lines, approaches a constant value because the corresponding partial decay widths are independent of neutrino masses while the decay length of Σ_3^0 diverges because it decays dominantly to WZh with the partial decay width proportional to m_3 . Similarly, $\Sigma_{1,2}^{\pm}$ decay is also dominated decay to WZh and is proportional to $m_{1,2}$, respectively. Therefore, the decay length $\Sigma_{1,2}^{\pm}$ approach the same constant value in the limit $m_3 \rightarrow 0$ because for the IH, $m_2 \rightarrow \sqrt{-\Delta m_{32}^2}$ and $m_1 \rightarrow \sqrt{-\Delta m_{32}^2 - \Delta m_{21}^2} \simeq \sqrt{-\Delta m_{32}^2}$.

Next, we consider the case $\theta_{1,2,3} \neq 0$. Let us parameterize $\theta_1 = x_1 + iy_1$, $\theta_2 = x_2 + iy_2$, and $\theta_3 = x_3 + iy_3$. In the following we set $x_{1,2,3} = 0$ for simplicity. In this case, $\cos(x_i + iy_i) \simeq \sin(x_i + iy_i) \simeq e^{y_i}$ for $y_i \gtrsim 1$. Hence,

$|R_{\alpha i}|^2$ can be exponentially enhanced for nonzero values of y_i . To see this effect, we consider Σ_i^{\pm} decay in Fig. 9 with $m_{\Sigma_{1(3)}} = 600$ GeV, $m_{\Sigma_{2,3(1,2)}} = 1$ TeV, respectively, and the angles $x_{1,2,3} = 0$ and $y_{1,2,3} = 10^{-3}$ (10^{-3}) for NH (IH). In this figure, for both NH and IH, curves corresponding to $\Sigma_{1,2,3}^{\pm/0}$ are depicted by solid, dashed and dotted lines. Also for both NH and IH, the red (blue) colored lines denote the branching ratio to WZh (Σ_0). The y_i values for the NH (IH) are chosen specifically to suppress the branching ratio of Σ_1^{\pm} (Σ_3^{\pm}) to WZh and also realize the lifetime for Σ^0 associated with the lightest observed neutrino, namely, Σ_1^0 (Σ_3^0) to be greater than 10 m.

For completeness, let us also consider the case with even larger y_i values. We show our results in Fig. 10 for $m_{\Sigma_{1(3)}} = 600$ GeV, $m_{\Sigma_{2,3(1,2)}} = 1$ TeV for NH (IH), respectively, with $x_{1,2,3} = 0$ and $y_{1,2,3} = 1$. The line codings for all the figures are the same as in Fig. 9. The branching ratio plots (top panel) shows that the decay of all triplets $\Sigma_{1,2,3}^{0,\pm}$, for both NH and IH, are dominated by their decay to WZh. In this case, the total decay width for both charged and neutral triplets in each Σ_i are identical as shown in Eqs. (4.1) and (4.3). Hence, the decay length of Σ_i^0 is same as that of Σ_i^{\pm} shown in the bottom

Fig. 9 For IH with $m_{\Sigma_1} = 600$ GeV, $m_{\Sigma_{2,3}} = 1$ TeV, $x_{1,2,3} = 0$ and $y_{1,2,3} = 10^{-3}$, the left panels show the branching ratio (top), decay length of Σ_i^\pm (middle) and Σ_i^0 (bottom) as a function of the lightest observed neutrino mass (m_3). All the line codings are the same as Fig. 7. The right panels show the same for the IH case, with $m_{\Sigma_3} = 600$ GeV, $m_{\Sigma_{1,2}} = 1$ TeV, $x_{1,2,3} = 0$ and $y_{1,2,3} = 10^{-3}$ as a function of m_3 and all the line codings are the same as Fig. 8



panels of Fig. 10. This shows that their decays are effectively prompt and therefore the choice of $m_{\Sigma_{1(3)}} = 600$ GeV for NH (IH) is inconsistent with the lower bound on promptly decaying triplet fermions of the type-III seesaw of 840 GeV.

In general, we find that all the triplet fermions, except for the one associated with the lightest observed neutrino ($\Sigma_{1(3)}$ for NH (IH), respectively), always decays promptly for all values of $y_i \geq 0$. See, for example, Figs. 7, 8, 9 and 10. Therefore, for NH (IH), $\Sigma_{1(3)}$ masses are subject to the CMS bound, namely, $m_{\Sigma_1} > 840$ GeV. For example, this excludes the IH scenario with $m_{\Sigma_1} = 600$ GeV and $m_{\Sigma_{2,3}} = 1$ TeV.

5 Prospect to search for fermion triplets at current/future colliders

In the previous section we have shown that the neutral lepton associated with the lightest observed neutrino, particularly

$\Sigma_{1(3)}^0$ for NH (IH), respectively, can have lifetime $c\tau \gg 10$ m and evade prompt detection at collider while their respective charged partners $\Sigma_{1(3)}^\pm$ have a much shorter lifetime and decay inside the detector. For the remainder of this paper, we will refer both of them as $\tilde{\Sigma}$ and their masses as $m_{\tilde{\Sigma}}$, which is effectively the same for both the charged and the neutral components of $\tilde{\Sigma}$. In this section, we will study the prospect to search for the disappearing track signature from $\tilde{\Sigma}^\pm$ decaying inside the LHC and the displaced vertex signature from $\tilde{\Sigma}^0$ decaying inside the MATHUSLA detector. We will also study the prospect to search for the displaced vertex signature from $\tilde{\Sigma}^\pm$ decaying inside the FCC-he.

5.1 Disappearing track searches for Σ^\pm at the LHC and HL-LHC

Although there is no dedicated LHC analysis of the disappearing track signature for the type-III seesaw, we can apply

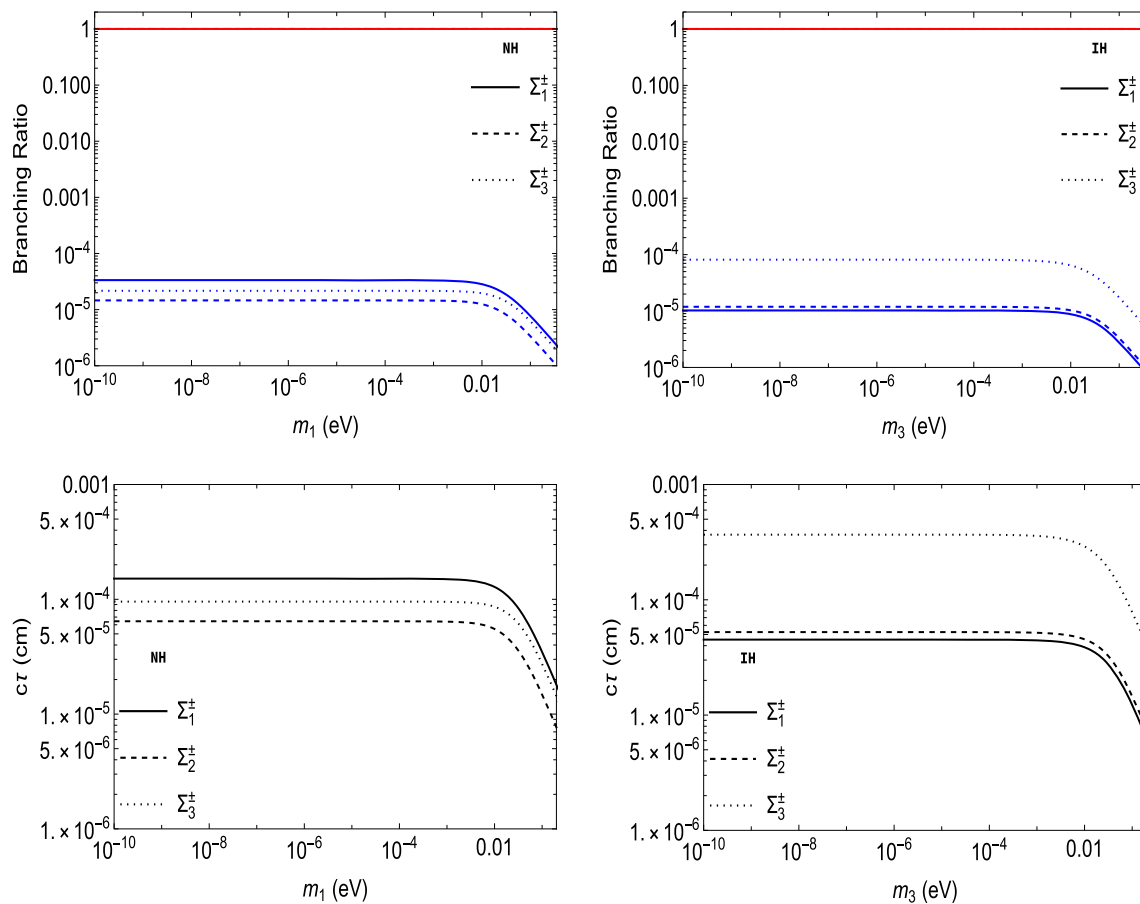


Fig. 10 For NH with $m_{\Sigma_1} = 600$ GeV, $m_{\Sigma_{2,3}} = 1$ TeV, $x_{1,2,3} = 0$ and $y_{1,2,3} = 1$, the left panels show the branching ratio (top) and decay length of Σ_i^\pm (middle) as a function of the lightest observed neutrino mass (m_1). All the line codings are the same as Fig. 7. The right panels show the same for the IH case, with $m_{\Sigma_3} = 600$ GeV, $m_{\Sigma_{1,2}} = 1$ TeV,

$x_{1,2,3} = 0$ and $y_{1,2,3} = 10^{-3}$ as a function of m_3 and all the line codings are the same as Fig. 8. For both NH and IH, the decay length of the neutral components is the same as the decay length of its charged partner. (See text for details)

the LHC search result for disappearing track signal from chargino decay [75, 76]. The CMS collaboration in Ref. [75] set an upper bound on the product of the production cross section (including both charged and neutral chargino) and its branching fraction of the chargino decaying to a neutralino plus a pion which is assumed to be 100%. Such a branching ratio is realized in the type-III seesaw in the limit $m_{1(3)} \rightarrow 0$ for NH (IH) as shown in Figs. 7, 8 and 9. In this limit, we can identify the bound in Ref. [75] as an upper bound on the total production cross section of $\tilde{\Sigma}^{0,\pm}$, which includes $\tilde{\Sigma}^0 \tilde{\Sigma}^\pm$ and $\tilde{\Sigma}^\mp \tilde{\Sigma}^\pm$ final states. We show our result in the left panel of Fig. 11, where the diagonal red line denotes the total production cross section for $\tilde{\Sigma}^{\pm,0}$ as a function of $m_{\tilde{\Sigma}}$. The red line in Fig. 11 is taken from the left panel of Fig. 4. The solid (dashed) black horizontal lines are the observed (expected) cross section limits from Ref. [75] while the green (yellow) band are expected 1(2)- σ upper limit on the production cross section. As indicated in the Fig. 11, this bound was obtained

for the chargino lifetime fixed to be 10 cm, which is longer than $c\tau_{\tilde{\Sigma}^\pm} \simeq 5$ cm⁵ for $\tilde{\Sigma}^\pm$ in the limit $m_{1(3)} \rightarrow 0$ for NH (IH), respectively.

In the right panel of Fig. 11 we show the decay length of $\tilde{\Sigma}^\pm$ along with the disappearing track search bound for wino-like chargino by the ATLAS collaboration [76] with 140 fb⁻¹ with the branching ratio of $\tilde{\Sigma}^\pm$ to $\tilde{\Sigma}^0$ fixed to be 95.5%. The solid horizontal black line depicts the decay length of $\tilde{\Sigma}^\pm$ for both NH (IH) and the benchmark values $\theta_{1,2,3} = 0$, $m_{\tilde{\Sigma}_1} = 600$ GeV, $m_{\Sigma_{2,3}}(m_{\Sigma_{1,2}}) = 1$ TeV and $m_{1(3)} = 10^{-9}$ eV, respectively. For the chosen benchmark values, the lines depicting decay length for NH and IH are completely overlapping and indistinguishable. The HL-LHC prospect in the right panel of Fig. 11 is obtained

⁵ This result was obtained by using the mass-splitting formula that only included one-loop contributions. Taking into account the two-loop contribution, the decay length of $\tilde{\Sigma}^\pm$ can increase by as much as 10% [77].

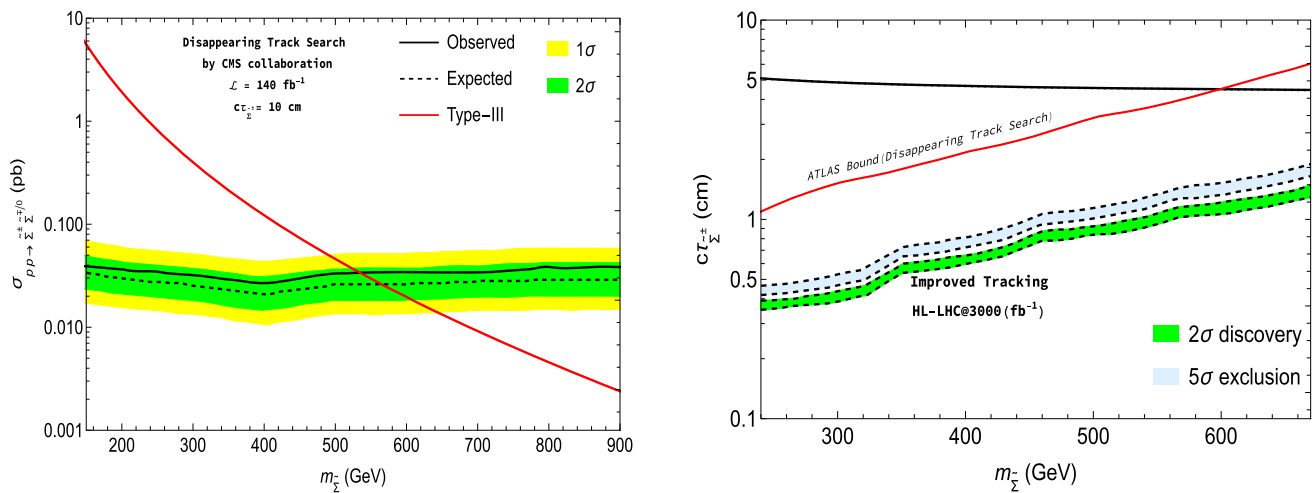


Fig. 11 The left panel shows the CMS bound on the production cross section of $\tilde{\Sigma}^\pm$ with lifetime $c\tau = 10$ cm as a function of its mass $m_{\tilde{\Sigma}}$. The solid (dashed) black horizontal lines are the observed (expected) limits on the cross section while the green (yellow) band are expected 1(2)- σ upper limit on the production cross section. The red diagonal line is our result for the total production cross section of the $\tilde{\Sigma}^\pm$ at

the LHC in Fig. 4. The right panel shows the prospect to search for $\tilde{\Sigma}^\pm$ disappearing track signature at high luminosity (HL)-LHC with 3000 fb^{-1} luminosity. The solid horizontal black line depict the decay length of $\tilde{\Sigma}^\pm$ for both NH (IH) for the benchmark values $\theta_{1,2,3} = 0$, $m_{\tilde{\Sigma}_1} = 600$ GeV, $m_{\Sigma_{2,3}}(m_{\Sigma_{1,2}}) = 1$ TeV and $m_{1(3)} = 10^{-9}$ eV

by re-interpreting the Higgsino disappearing track search prospect in Ref. [79] (namely, Fig. 9(c)) with the assumption of “improved detector tracking”. To obtain the bound, we take into consideration various similarities and differences between the production and decay of Higgsino and the type-III seesaw triplets. The production processes of $\tilde{\Sigma}^\pm$ ($\tilde{\Sigma}^0$) are the same as the charged (neutral) components of Higgsino whereas their production rates differ due to their $SU(2)_L$ representations, namely, Higgsino belong to the $SU(2)_L$ doublet while $\tilde{\Sigma}$ is $SU(2)_L$ triplet. Unlike the triplets, the Higgsino (charged and neutral) do not decay to WZ h at the tree-level. In the type-III seesaw case, this can be achieved in the limiting case $m_{1(3)} \rightarrow 0$ for NH (IH). On the other hand, the charged Higgsino decays to neutral Higgsino plus soft pions/SM leptons is the same as $\tilde{\Sigma}^\pm$ decay. However, the decay length of a charged Higgsino is essentially a free parameter because the mass-splitting between the charged and neutral Higgsinos, which determines the decay length, is a free parameter in the supersymmetric SM. In the type-III seesaw case, the decay length depends on the mass-splitting, which is fixed to be around the pion mass, and neutrino oscillation parameters as we have shown in the previous section. Taking into account all these factors, we can conclude that there is a one-to-one correspondence between the production rate of Higgsino and $\tilde{\Sigma}$ (for a fixed value of mass) that results in a one-to-one correspondence between the Higgsino mass, its production rate and lifetime in Ref. [79]. It is worth noting that the authors in Ref. [79] also show the HL-LHC prospect with “standard tracking” assumptions and 3000 fb^{-1} luminosity. Interestingly, we found that the current ATLAS bound is already is

comparable if not better than the “standard tracking” prospect. Hence, we expect the HL-LHC with 3000 fb^{-1} luminosity to perform significantly better than the prospect shown in the right panel of Fig. 11.

5.2 Displaced vertex search for Σ^0 at MATHUSLA

The recently, proposed MATHUSLA [50] is purposefully designed to detect neutral long-lived particles produced at the LHC, and will be located ~ 100 m away from the beam collision point with an angle $\theta = [0.38, 0.8]$ from the LHC beam direction. Hence, it is ideally suited to detect long-lived particles with their decay lengths in the range of few hundred meters or even longer [80]. If the particle decays with final state charged leptons and/or jets, the event can be easily reconstructed because the background SM events will be almost zero.

As shown in Fig. 7 (Fig. 8), the decay length of $\tilde{\Sigma}^0$ corresponding to NH (IH), respectively, have decay length of 100 m for the benchmark values $\theta_{1,2,3} = 0$, $m_{\tilde{\Sigma}_1} = 600$ GeV, $m_{\Sigma_{2,3}}(m_{\Sigma_{1,2}}) = 1$ TeV and $m_{1(3)} = 10^{-9}$ eV. In the following, we investigate a possibility of detecting $\tilde{\Sigma}^0$ at MATHUSLA. At LHC, $\tilde{\Sigma}^0$ is produced in two ways. One is from $\tilde{\Sigma}^\pm$ production through a s -channel Z/γ in the left diagram of Fig. 3, and the other is through s -channel W^\pm exchange process in the middle diagram of Fig. 3. In the first case, $\tilde{\Sigma}^0$ is produced by $\tilde{\Sigma}^\pm$ decay while in the other one $\tilde{\Sigma}^0$ is directly produced. The other particles produced from $\tilde{\Sigma}^\pm$ decay are soft and will not be considered in our analysis. Since the MATHUSLA detector is very efficient in detecting

long-lived particles, we will simply require that $\tilde{\Sigma}^0$ particle produced at the LHC reaches the MATHUSLA detector and decays inside the detector. In the following, we assume that the decaying $\tilde{\Sigma}^0$ particle can be detected with 100% efficiency by MATHUSLA because the SM backgrounds are expected to be negligible.

Let us assume that $\tilde{\Sigma}^0$ produced at the LHC is emitted at an angle of θ away from the LHC beam line such that it decays after traveling a distance of D_M . The decay length in the laboratory frame is given by

$$c\tau_{\text{lab}} = \frac{D_M}{\beta}. \quad (5.1)$$

Here, the β is the boost factor for $\tilde{\Sigma}^0$ particle,

$$\beta = \frac{1}{\sqrt{1 + \frac{m_{\tilde{\Sigma}^0}^2}{\vec{P}_{\text{tot}}^2}}}, \quad (5.2)$$

with a total momentum $\vec{P}_{\text{tot}} = p_T \cosh \eta$, where p_T is $\tilde{\Sigma}^0$'s transverse momentum and $\eta = -\ln[\tan(\theta/2)]$ is its rapidity. Hence, the proper decay length of $\tilde{\Sigma}^0$ is given by

$$c\tau_{\tilde{\Sigma}^0} = c\tau_{\text{lab}} \times \sqrt{1 - \beta^2} = D_M \frac{\sqrt{1 - \beta^2}}{\beta}. \quad (5.3)$$

We fix $D_M = 100$ m and set $\theta \simeq 0.5$ corresponding to the location of the MATHUSLA detector. Hence, $P_{\text{tot}} \simeq 2p_T$ and

$$c\tau_{\tilde{\Sigma}^0} \simeq 2D_M \left(\frac{m_{\tilde{\Sigma}^0}}{p_T} \right) = 200 \left(\frac{m_{\tilde{\Sigma}^0}}{p_T} \right). \quad (5.4)$$

To simulate the production of $\tilde{\Sigma}^0$ observed by MATHUSLA, we employ MADGRAPH5AMC @NLO [74,78] and calculate the production cross section (σ) for the process. Since $c\tau_{\tilde{\Sigma}^\pm} \simeq 5$ cm for our benchmark is smaller than the benchmark value of 9 cm used in the Higgsino search analysis, we expect the lower-bound on $\tilde{\Sigma}^0$ mass to be weaker than $m_{\tilde{\Sigma}^0} \simeq 380$ GeV shown in the left panel of Fig. 11. Thus, in the following, we consider two benchmark values, $m_{\tilde{\Sigma}^0} = 600$ (700) GeV. In the top left (right) panel of Fig. 12, for $m_{\tilde{\Sigma}^0} = 600$ (700) GeV, we show the cross section as a function of transverse momentum (p_T) of $\tilde{\Sigma}^0$. Because of low background, let us require 25 events ($N = 25$) for a “ $\tilde{\Sigma}^0$ discovery” at MATHUSLA. In the bottom left (right) panel of Fig. 12, for $m_{\tilde{\Sigma}^0} = 600$ (700) GeV, we show the luminosity ($\mathcal{L} = N/\sigma$) required for the discovery of $\tilde{\Sigma}^0$ as a function of its decay length, which we evaluated by using Eq. (5.4). The bottom (top) horizontal line denotes the integrated luminosity at HL-LHC with $\mathcal{L} = 300$ (3000) fb^{-1} . From the bottom panels we find that the MATHUSLA can discover $\tilde{\Sigma}^0$ with a mass 600 GeV and 700 GeV, if their decay lengths are in the range $\mathcal{O}(10^2)$ m– $\mathcal{O}(10^4)$ m for both the cases. Since the cross section decreases with increasing $m_{\tilde{\Sigma}}$ values, a heavier

$\tilde{\Sigma}_0$ requires a higher luminosity. For example, we find that $m_{\tilde{\Sigma}^0} = 1000$ GeV requires $\mathcal{L} > 3000$ fb^{-1} for any $c\tau$ values.

5.3 Displaced vertex searches for Σ^\pm at FCC-he

Let us now consider the displaced vertex signature arising from $\tilde{\Sigma}^\pm$ decay at ep -colliders.⁶ Authors in Ref. [55] have studied the prospect to detect charged Higgsinos at FCC-he experiment to show that these experiments can probe much shorter decay length, 10^{-3} –10 cm, compared to the pp -colliders. As in the case of HL-LHC, we can recast their search prospect by exploiting the one-to-one correspondence between the Higgsino mass, its production rate and lifetime while taking into account the differences in the production rate of Higgsino and $\tilde{\Sigma}$. Because the charged Higgsino decays 100% to the long-lived neutral Higgsino that evades detection and soft pion/SM leptons, the results in Ref. [55] is only applicable to the type-III seesaw in the limiting case $m_{1(3)} \rightarrow 0$ for NH (IH). See, for example, Figs. 7 and 8. Particularly, we fix $m_{1(3)} = 10^{-9}$ eV for the following analysis.

Employing the prospect for detecting the long-lived charged Higgsino presented in Ref. [55], in the left panel of Fig. 13 we show the prospects for FCC-he with 1 ab^{-1} luminosity. The blue and green shaded regions indicate the parameter space where 100 (10) events with at least one long-lived Σ^\pm is observed at the FCC-he; the green shaded regions correspond to 2- σ exclusion sensitivity. In the right panel, the red shaded regions 2- σ exclusion sensitivity if the backgrounds are harder to reject. The grey shaded region in all the plots is excluded for the long-lived Higgsino scenario but is still allowed in our scenario. In each panels of Fig. 13, we also show the 5- σ exclusion reach of HL-LHC obtained in the right panel of Fig. 11 from the disappearing track searches. We also show the decay length of $\tilde{\Sigma}^\pm$ corresponding to NH (IH), which are both depicted by the horizontal black line for the benchmark values $\theta_{1,2,3} = 0$, $m_{\tilde{\Sigma}} = 600$ GeV and $m_{\Sigma_{2,3}}(m_{\Sigma_{1,2}}) = 1$ TeV and $m_{1(3)} = 10^{-9}$ eV, respectively.

6 Summary

We have investigated the prospect of probing the type III seesaw neutrino mass generation mechanism at various collider experiments by searching for a disappearing track signature as well as a displaced vertex signature originating from the decay of $SU(2)_L$ triplet fermion Σ . We consider scenario with three triplet fermions, $\Sigma_{i=1,2,3}$, each of which include one neutral component, Σ^0 , and two charged components, Σ^\pm . Because Σ_i is primarily produced at colliders through

⁶ The prospect for probing the type-I seesaw scenario at LHeC has been investigated in Ref. [81] with prompt decays of the right-handed neutrinos.

Fig. 12 The top left (right) show the production cross section as a function of p_T for $m_{\tilde{\Sigma}} = 600$ (700) GeV. In the bottom panels, we show the luminosities required to produce 25 $\tilde{\Sigma}$ at LHC which are directed towards MATHUSLA, and the horizontal bottom (top) line denote $\mathcal{L} = 300$ (3000) fb^{-1}

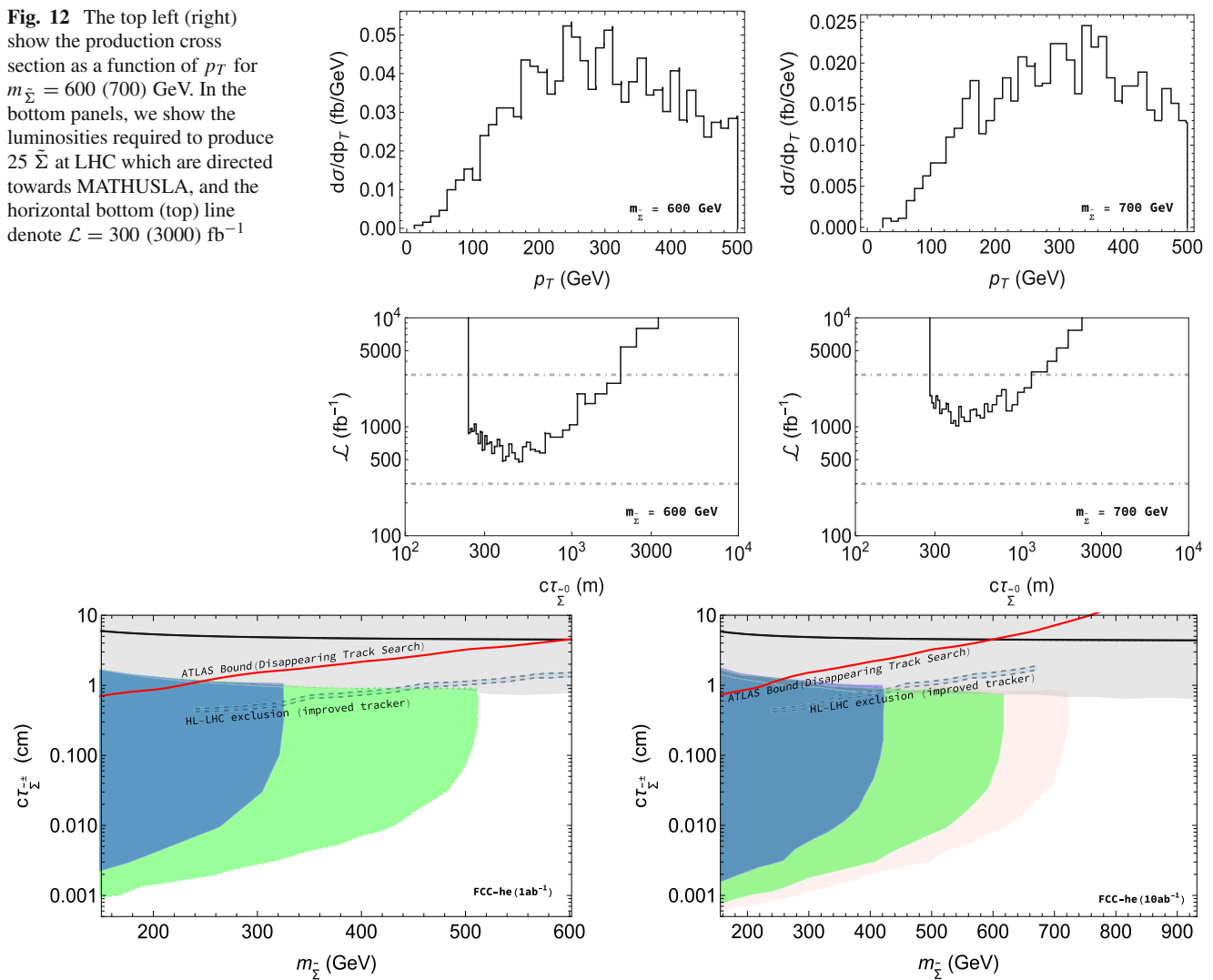


Fig. 13 The plots show the prospects of observing displaced vertex from Σ^\pm decay at FCC-he. The blue and green shaded regions indicate the parameter space where 100 (10) events with at least one long-lived Σ^\pm . The light-red shaded region indicate 2- σ exclusion sensitivity if the backgrounds are harder to reject. The grey shaded region are still

allowed in our type-III seesaw scenario. The solid horizontal black line depict the decay length of $\tilde{\Sigma}^\pm$ for both NH (IH) and the benchmark values $\theta_{1,2,3} = 0$, $m_{\tilde{\Sigma}} = 600$ GeV and $m_{\Sigma_{2,3}}(m_{\Sigma_{1,2}}) = 1$ TeV and $m_{1(3)} = 10^{-9}$ eV, respectively

their electroweak gauge interactions, its production rate is uniquely determined by its mass m_{Σ_i} . The type-III seesaw mechanism generates the observed neutrinos masses, which together with m_{Σ_i} , determine the decay length of $\Sigma_i^{0,\pm}$. We have shown that the neutral lepton associated with the lightest observed neutrino, particularly $\Sigma_{1(3)}^0$ for NH (IH), respectively, can have lifetime $c\tau \gg 10$ m and evade detection at collider while their respective charged partners $\Sigma_{1(3)}^\pm$ have a much shorter lifetime and decay inside the detector. The $\Sigma_{1(3)}^\pm$ with a mass few hundred GeV and associated with the lightest observed neutrino $m_{1(3)}$ for NH (IH), respectively, decay and produce a disappearing track signature which can be searched at future pp -collider such as the HL-LHC. If the

lightest observed neutrino, $m_{1(3)}$ for NH (IH), respectively, has mass around 10^{-9} eV, we have shown that both $\Sigma_{1(3)}^0$ have a decay length of around 100 m and can be discovered at the proposed MATHUSLA detector. On the other hand, for NH (IH), we have also shown that $\Sigma_{1(3)}^\pm$, respectively, decay to produce an observable displaced vertex signature at the FCC-he.

Acknowledgements We thank Oliver Fischer for helpful discussions. This work is supported in part by the United States Department of Energy grant de-sc0012447 (N.O) and de-sc0013880 (D.R).

Data Availability Statement This manuscript has no associated data or the data will not be deposited. [Authors' comment: All the result

shown in this work can be reproduced using the formulas listed in the paper.]

Open Access This article is licensed under a Creative Commons Attribution 4.0 International License, which permits use, sharing, adaptation, distribution and reproduction in any medium or format, as long as you give appropriate credit to the original author(s) and the source, provide a link to the Creative Commons licence, and indicate if changes were made. The images or other third party material in this article are included in the article's Creative Commons licence, unless indicated otherwise in a credit line to the material. If material is not included in the article's Creative Commons licence and your intended use is not permitted by statutory regulation or exceeds the permitted use, you will need to obtain permission directly from the copyright holder. To view a copy of this licence, visit <http://creativecommons.org/licenses/by/4.0/>.

Funded by SCOAP³. SCOAP³ supports the goals of the International Year of Basic Sciences for Sustainable Development.

References

- Q.R. Ahmad et al. (SNO Collaboration), Phys. Rev. Lett. **89**, 011301 (2002). [arXiv:nucl-ex/0204008](#)
- Q.R. Ahmad et al. (SNO Collaboration), Phys. Rev. Lett. **89**, 011302 (2002). [arXiv:nucl-ex/0204009](#)
- J. Hosaka et al. (Super-Kamiokande Collaboration), Phys. Rev. D **74**, 032002 (2006). [arXiv:hep-ex/0604011](#)
- K. Eguchi et al. (KamLAND Collaboration), Phys. Rev. Lett. **90**, 021802 (2003). [arXiv:hep-ex/0212021](#)
- M.H. Ahn et al. (K2K Collaboration), Phys. Rev. Lett. **90**, 041801 (2003). [arXiv:hep-ex/0212007](#)
- K. Abe et al. (T2K Collaboration), Phys. Rev. Lett. **107**, 041801 (2011). [arXiv:1106.2822](#) [hep-ex]
- P. Minkowski, Phys. Lett. B **67**, 421 (1977)
- T. Yanagida, in *Proceedings of the Workshop on the Unified Theory and the Baryon Number in the Universe*, ed. by O. Sawada et al., p. 95, KEK Report 79-18, Tsukuba (1979)
- M. Gell-Mann, P. Ramond, R. Slansky, in *Supergravity*, ed. by P. van Nieuwenhuizen et al., (North-Holland, 1979), p. 315
- S.L. Glashow, in *Quarks and Leptons, Cargèse*, ed. by M. Lévy et al. (Plenum, 1980), p. 707
- R.N. Mohapatra, G. Senjanović, Phys. Rev. Lett. **44**, 912 (1980)
- W. Konetschny, W. Kummer, Phys. Lett. B **70**, 433 (1977)
- T.P. Cheng, L.F. Li, Phys. Rev. D **22**, 2860 (1980)
- G. Lazarides, Q. Shafi, C. Wetterich, Nucl. Phys. B **181**, 287 (1981)
- J. Schechter, J.W.F. Valle, Phys. Rev. D **22**, 2227 (1980)
- R.N. Mohapatra, G. Senjanović, Phys. Rev. D **23**, 165 (1981)
- R. Foot, H. Lew, X.G. He, G.C. Joshi, Z. Phys. C **44**, 441 (1989)
- E. Ma, Phys. Rev. Lett. **81**, 1171 (1998). [arXiv:hep-ph/9805219](#)
- B. Bajc, G. Senjanović, JHEP **0708**, 014 (2007). [arXiv:hep-ph/0612029](#)
- P. Fileviez Pérez, Phys. Lett. B **654**, 189 (2007)
- P. Fileviez Pérez, Phys. Rev. D **76** (2007) 071701. [arXiv:0705.3589](#) [hep-ph]
- F. del Aguila, J.A. Aguilar-Saavedra, Nucl. Phys. B **813**, 22 (2009). [arXiv:0808.2468](#) [hep-ph]
- R. Franceschini, T. Hambye, A. Strumia, Type-III see-saw at LHC. Phys. Rev. D **78**, 033002 (2008). [arXiv:0805.1613](#) [hep-ph]
- B. Bajc, M. Nemevsek, G. Senjanovic, Probing seesaw at LHC. Phys. Rev. D **76**, 055011 (2007). [arXiv:hep-ph/0703080](#) [hep-ph]
- A. Arhrib, B. Bajc, D.K. Ghosh, T. Han, G.Y. Huang, I. Puljak, G. Senjanovic, Collider signatures for heavy lepton triplet in type I+III seesaw. Phys. Rev. D **82**, 053004 (2010). [arXiv:0904.2390](#) [hep-ph]
- P. Bandyopadhyay, S. Choi, E.J. Chun, K. Min, Probing Higgs bosons via the type III seesaw mechanism at the LHC. Phys. Rev. D **85**, 073013 (2012). [arXiv:1112.3080](#) [hep-ph]
- D. Goswami, P. Poulose, Direct searches of Type III seesaw triplet fermions at high energy e^+e^- collider. Eur. Phys. J. C **78**(1), 42 (2018). [arXiv:1702.07215](#) [hep-ph]
- A. Biswas, D. Borah, D. Nanda, When freeze-out precedes freeze-in: sub-TeV fermion triplet dark matter with radiative neutrino mass. JCAP **1809**, 014 (2018). [arXiv:1806.01876](#) [hep-ph]
- A. Biswas, D. Borah, D. Nanda, Type III seesaw for neutrino masses in $U(1)_{B-L}$ model with multi-component dark matter. [arXiv:1908.04308](#) [hep-ph]
- A.M. Sirunyan et al. (CMS Collaboration), Search for evidence of the type-III seesaw mechanism in dilepton final states in proton–proton collisions at $\sqrt{s} = 13$ TeV. Phys. Rev. Lett. **119**(22), 221802 (2017). [arXiv:1708.07962](#) [hep-ex]
- The ATLAS Collaboration (ATLAS Collaboration), Search for type-III seesaw heavy leptons in proton–proton collisions at $\sqrt{s} = 13$ TeV with the ATLAS detector. ATLAS-CONF-2018-020
- M. Aaboud et al. (ATLAS Collaboration), Search for long-lived charginos based on a disappearing-track signature in pp collisions at $\sqrt{s} = 13$ TeV with the ATLAS detector. JHEP **1806**, 22 (2018). [arXiv:1712.02118](#) [hep-ex]
- G. Aad et al. (ATLAS Collaboration), Search for a light Higgs boson decaying to long-lived weakly-interacting particles in proton–proton collisions at $\sqrt{s} = 7$ TeV with the ATLAS detector. Phys. Rev. Lett. **108**, 251801 (2012)
- S. Chatrchyan et al. (CMS Collaboration), Search for heavy long-lived charged particles in pp collisions at $\sqrt{s} = 7$ TeV
- G. Aad et al. (ATLAS Collaboration), Search for displaced muonic lepton jets from light Higgs boson decay in proton–proton collisions at $\sqrt{s} = 7$ TeV with the ATLAS detector. Phys. Lett. B **721**, 32 (2013). [arXiv:1210.0435](#) [hep-ex]
- G. Aad et al. (ATLAS Collaboration), Search for long-lived, heavy particles in final states with a muon and multi-track displaced vertex in proton–proton collisions at $\sqrt{s} = 7$ TeV with the ATLAS detector. Phys. Lett. B **719**, 280 (2013). [arXiv:1210.7451](#) [hep-ex]
- S. Chatrchyan et al. (CMS Collaboration), Search in leptonic channels for heavy resonances decaying to long-lived neutral particles. JHEP **1302**, 085 (2013). [arXiv:1211.2472](#) [hep-ex]
- G. Aad et al. (ATLAS Collaboration), Search for long-lived neutral particles decaying into lepton jets in proton–proton collisions at $\sqrt{s} = 8$ TeV with the ATLAS detector. JHEP **1411**, 088 (2014). [arXiv:1409.0746](#) [hep-ex]
- V. Khachatryan et al. (CMS Collaboration), Search for long-lived neutral particles decaying to quark–antiquark pairs in proton–proton collisions at $\sqrt{s} = 8$ TeV. Phys. Rev. D **91**(1), 012007 (2015). [arXiv:1411.6530](#) [hep-ex]
- V. Khachatryan et al. (CMS Collaboration), Search for long-lived particles that decay to final states containing two electrons or two muons in proton–proton collisions at $\sqrt{s} = 8$ TeV. Phys. Rev. D **91**(5), 052012 (2015). [arXiv:1411.6977](#) [hep-ex]
- R. Aaij et al. (LHCb Collaboration), Search for long-lived particles decaying to jet pairs. Eur. Phys. J. C **75**(4), 152 (2015). [arXiv:1412.3021](#) [hep-ex]
- G. Aad et al. (ATLAS Collaboration), Search for pair-produced long-lived neutral particles decaying in the ATLAS hadronic calorimeter in pp collisions at $\sqrt{s} = 8$ TeV. Phys. Lett. B **743**, 15 (2015). [arXiv:1501.04020](#) [hep-ex]
- G. Aad et al. (ATLAS Collaboration), Search for long-lived, weakly interacting particles that decay to displaced hadronic jets in proton–proton collisions at $\sqrt{s} = 8$ TeV with the ATLAS detector. Phys. Rev. D **92**(1), 012010 (2015). [arXiv:1504.03634](#) [hep-ex]
- G. Aad et al. (ATLAS Collaboration), Search for massive, long-lived particles using multitrack displaced vertices or displaced lep-

- ton pairs in pp collisions at $\sqrt{s} = 8$ TeV with the ATLAS detector. Phys. Rev. D **92**(7), 072004 (2015). [arXiv:1504.05162](#) [hep-ex]
45. M. Aaboud et al. (ATLAS Collaboration), Search for metastable heavy charged particles with large ionization energy loss in pp collisions at $\sqrt{s} = 13$ TeV using the ATLAS experiment. Phys. Rev. D **93**(11), 112015 (2016). [arXiv:1604.04520](#) [hep-ex]
 46. M. Aaboud et al. (ATLAS Collaboration), Search for heavy long-lived charged R -hadrons with the ATLAS detector in 3.2 fb^{-1} of proton–proton collision data at $\sqrt{s} = 13$ TeV. Phys. Lett. B **760**, 647 (2016). [arXiv:1606.05129](#) [hep-ex]
 47. The ATLAS Collaboration (ATLAS Collaboration), Search for long-lived neutral particles decaying into displaced lepton jets in proton–proton collisions at $\sqrt{s} = 13$ TeV with the ATLAS detector. ATLAS-CONF-2016-042
 48. The ATLAS Collaboration (ATLAS Collaboration), Search for long-lived neutral particles decaying in the hadronic calorimeter of ATLAS at $\sqrt{s} = 13$ TeV in 3.2 fb^{-1} of data. ATLAS-CONF-2016-103
 49. M. Aaboud et al. (ATLAS Collaboration), Search for long-lived, massive particles in events with displaced vertices and missing transverse momentum in $\sqrt{s} = 13$ TeV pp collisions with the ATLAS detector. Phys. Rev. D **97**(5), 052012 (2018). [arXiv:1710.04901](#) [hep-ex]
 50. J.P. Chou, D. Curtin, H.J. Lubatti, New detectors to explore the lifetime frontier. Phys. Lett. B **767**, 29 (2017). [arXiv:1606.06298](#) [hep-ph]
 51. A. Ariga et al. (FASER Collaboration), Phys. Rev. D **99**(9), 095011 (2019). [arXiv:1811.12522](#) [hep-ph]
 52. D. Dercks, J. De Vries, H.K. Dreiner, Z.S. Wang, Phys. Rev. D **99**(5), 055039 (2019). [arXiv:1810.03617](#) [hep-ph]
 53. J.L. Abelleira Fernandez et al. (LHeC Study Group), A large hadron electron collider at CERN report on the physics and design concepts for machine and detector. J. Phys. G **39**, 075001 (2012). [arXiv:1206.2913](#) [physics.acc-ph]
 54. M. Kuze, Energy-frontier lepton-hadron collisions at CERN: the LHeC and the FCC-he
 55. D. Curtin, K. Deshpande, O. Fischer, J. Zurita, New physics opportunities for long-lived particles at electron–proton colliders. JHEP **1807**, 024 (2018). [arXiv:1712.07135](#) [hep-ph]
 56. S. Jana, N. Okada, D. Raut, Displaced vertex signature of type-I seesaw model. Phys. Rev. D **98**(3), 035023 (2018). [arXiv:1804.06828](#) [hep-ph]
 57. J.C. Helo, M. Hirsch, S. Kovalenko, Heavy neutrino searches at the LHC with displaced vertices. Phys. Rev. D **89**, 073005 (2014). [arXiv:1312.2900](#) [hep-ph]. [Erratum: Phys. Rev. D **93**(9), 099902 (2016)]
 58. G. Cottin, J.C. Helo, M. Hirsch, Searches for light sterile neutrinos with multitrack displaced vertices. Phys. Rev. D **97**(5), 055025 (2018). [arXiv:1801.02734](#) [hep-ph]
 59. G. Cottin, J.C. Helo, M. Hirsch, Displaced vertices as probes of sterile neutrino mixing at the LHC. Phys. Rev. D **98**(3), 035012 (2018). [arXiv:1806.05191](#) [hep-ph]
 60. D. Curtin et al., Long-lived particles at the energy frontier: the MATHUSLA physics case. [arXiv:1806.07396](#) [hep-ph]
 61. D. Dercks, H.K. Dreiner, M. Hirsch, Z.S. Wang, Long-lived fermions at AL3X. Phys. Rev. D **99**(5), 055020 (2019). [arXiv:1811.01995](#) [hep-ph]
 62. G. Cottin, J.C. Helo, M. Hirsch, D. Silva, Revisiting the LHC reach in the displaced region of the minimal left-right symmetric model. [arXiv:1902.05673](#) [hep-ph]
 63. C.W. Chiang, G. Cottin, A. Das, S. Mandal, Displaced heavy neutrinos from Z' decays at the LHC. [arXiv:1908.09838](#) [hep-ph]
 64. C. Arbeláez, J.C. Helo, M. Hirsch, Long-lived heavy particles in neutrino mass models. Phys. Rev. D **100**(5), 055001 (2019). [arXiv:1906.03030](#) [hep-ph]
 65. A. Das, P.S.B. Dev, N. Okada, Long-lived TeV-scale right-handed neutrino production at the LHC in gauged $U(1)_X$ model. Phys. Lett. B **799**, 135052 (2019). [arXiv:1906.04132](#) [hep-ph]
 66. S. Antusch, O. Fischer, A. Hammad, Lepton-trijet and displaced vertex searches for heavy neutrinos at future electron–proton colliders. [arXiv:1908.02852](#) [hep-ph]
 67. M. Cirelli, N. Fornengo, A. Strumia, Minimal dark matter. Nucl. Phys. B **753**, 178 (2006). [arXiv:hep-ph/0512090](#)
 68. M. Tanabashi et al. (Particle Data Group), Review of particle physics. Phys. Rev. D **98**(3), 030001 (2018)
 69. I. Esteban, M.C. Gonzalez-Garcia, M. Maltoni, T. Schwetz, A. Zhou, The fate of hints: updated global analysis of three-flavor neutrino oscillations. JHEP **09**, 178 (2020). [arXiv:2007.14792](#) [hep-ph]
 70. J.A. Casas, A. Ibarra, Oscillating neutrinos and $\mu \rightarrow e, \gamma$. Nucl. Phys. B **618**, 171 (2001). [arXiv:hep-ph/0103065](#)
 71. K. Ghosh, S. Jana, S. Nandi, Neutrino mass generation at TeV scale and new physics signatures from charged Higgs at the LHC for photon initiated processes. JHEP **1803**, 180 (2018). [arXiv:1705.01121](#) [hep-ph]
 72. K.S. Babu, S. Jana, Probing doubly charged Higgs bosons at the LHC through photon initiated processes. Phys. Rev. D **95**(5), 055020 (2017). [arXiv:1612.09224](#) [hep-ph]
 73. T. Ghosh, S. Jana, S. Nandi, Neutrino mass from Higgs quadruplet and multicharged Higgs searches at the LHC. Phys. Rev. D **97**(11), 115037 (2018). [arXiv:1802.09251](#) [hep-ph]
 74. J. Alwall, M. Herquet, F. Maltoni, O. Mattelaer, T. Stelzer, MadGraph 5: going beyond. JHEP **1106**, 128 (2011). [arXiv:1106.0522](#) [hep-ph]
 75. A.M. Sirunyan et al. (CMS), Search for disappearing tracks in proton–proton collisions at $\sqrt{s} = 13$ TeV. Phys. Lett. B **806**, 135502 (2020). [arXiv:2004.05153](#) [hep-ex]
 76. G. Aad et al. (ATLAS), Search for long-lived charginos based on a disappearing-track signature using 136 fb^{-1} of pp collisions at $\sqrt{s} = 13$ TeV with the ATLAS detector. Eur. Phys. J. C **82**(7), 606 (2022). [arXiv:2201.02472](#) [hep-ex]
 77. M. Ibe, S. Matsumoto, R. Sato, Mass splitting between charged and neutral winos at two-loop level. Phys. Lett. B **721**, 252–260 (2013). [arXiv:1212.5989](#) [hep-ph]
 78. J. Alwall et al., The automated computation of tree-level and next-to-leading order differential cross sections, and their matching to parton shower simulations. JHEP **1407**, 079 (2014). [arXiv:1405.0301](#) [hep-ph]
 79. R. Mahbubani, P. Schwaller, J. Zurita, Closing the window for compressed Dark Sectors with disappearing charged tracks. JHEP **1706**, 119 (2017). [arXiv:1703.05327](#) [hep-ph]. [Erratum: JHEP **1710**, 061 (2017)]
 80. D. Curtin, M.E. Peskin, Analysis of long lived particle decays with the MATHUSLA detector. Phys. Rev. D **97**(1), 015006 (2018). [arXiv:1705.06327](#) [hep-ph]
 81. A. Das, S. Jana, S. Mandal, S. Nandi, Probing right handed neutrinos at the LHeC and lepton colliders using fat jet signatures. Phys. Rev. D **99**(5), 055030 (2019). [arXiv:1811.04291](#) [hep-ph]